The boron and lithium isotopic composition of mid-ocean ridge basalts and the mantle

Horst Marschall (WHOI; Frankfurt), **Dorsey Wanless** (Boise State University)
Nobumichi Shimizu (WHOI), **Philip Pogge von Strandmann** (UCL and Birkbeck, University of London)
Brian Monteleone (WHOI), **Tim Elliott** (University of Bristol)

Accuracy of Li isotope analyses

The reproducibility cited in Elliott *et al.* (2006) was based on repeat analyses of international reference materials over several years, reported in detail in Jeffcoate *et al.* (2004), but further supplemented in Elliott *et al.* (2006) with additional measurements of BHVO-2 and two full MORB replicate analyses. These data indicated a reproducibility of 0.3‰ (2SD). Evidently the samples remeasured here do not reproduce within this original assessment of errors (Fig. S1).

There are several potential causes of this discrepancy. We believe the most likely is subtle changes in analytical routines of different users. We have found that the variability of δ^7Li for the same silicate standards analysed by different users can be greater than the reproducibility by the same user. From the Bristol laboratory, the greatest amount of δ^7Li data have been collected by Pogge von Strandmann, the analyst of the repeat MORB measurements reported in this contribution. The values of several reference materials obtained by this user were reported in Pogge von Strandmann *et al.* (2011). A more recent compilation of

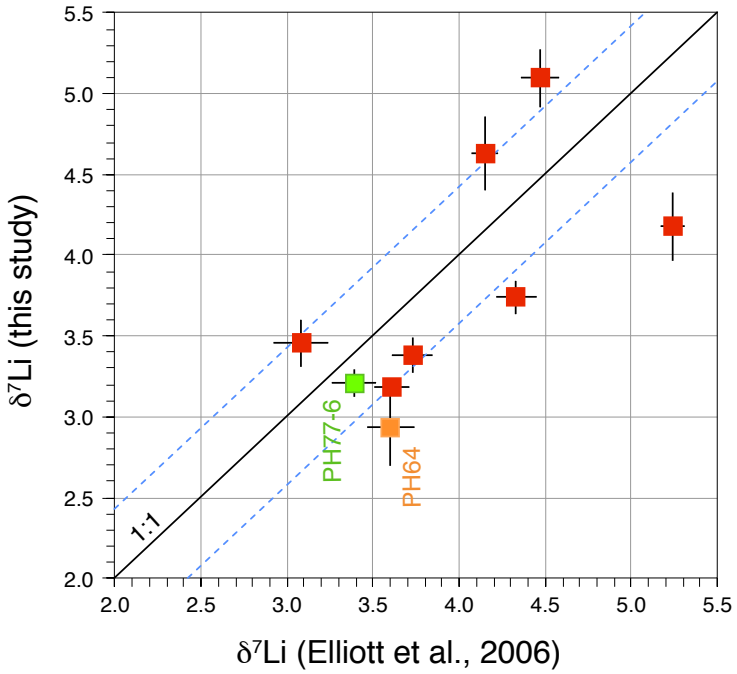

Fig. S 1 Lithium isotope analyses of EPR MORB glass samples analysed in this study plotted against analyses of the same samples published in Elliott *et al.* (2006). The stippled lines delimit a propagated error of the difference of two analyses each with a precision of 0.3‰. 9 mg of glass was used for PH64, whereas only 2 mg was picked of PH77.

Table S 1 Lithium isotope analyses of basaltic reference materials at Bristol, 2006–2015

BHVO-2			BCR-2			JB-2		
δ^7Li (‰)	2SD	analysis date	δ^7Li (‰)	2SD	analysis date	δ^7Li (‰)	2SD	analysis date
+4.66	0.65	25.10.2006	+2.58	0.69	29.09.2006	+5.10	0.13	25.10.2006
+4.82	1.06	25.10.2006	+2.83	0.31	25.10.2006	+4.95	0.18	25.10.2006
+4.94	0.53	26.10.2006	+2.58	0.54	20.11.2006	+4.80	0.70	26.10.2006
+4.65	0.54	26.10.2006	+2.65	0.25	09.03.2007	+4.81	0.03	06.11.2006
+4.58	0.00	26.10.2006	+2.70	0.35	21.06.2007	+4.96	0.14	06.11.2006
+4.71	0.10	26.10.2006	+2.43	0.19	25.07.2007	+5.01	0.24	15.11.2006
+4.80	0.21	06.11.2006	+2.70	0.09	09.11.2007	+4.88	0.55	15.11.2006
+4.69	0.13	06.11.2006	+2.53	0.50	22.10.2008	*+5.11*	*0.32*	20.11.2006
+4.82	0.44	11.12.2006	+2.56	0.08	26.11.2008	+4.58	0.25	25.11.2006
+4.78	*0.17*	30.01.2007	+2.61	0.07	12.12.2008	*+4.95*	*0.27*	04.12.2006
+4.69	0.77	02.02.2007	+2.40	0.19	03.03.2009	+5.10	0.13	02.02.2007
+4.92	0.11	08.02.2007	*+2.34*	*0.10*	29.09.2010	*+4.98*	*0.18*	02.02.2007
+4.72	*0.18*	09.03.2007	+2.49	0.25	08.12.2010	+5.14	0.31	10.07.2007
+4.84	*0.45*	09.03.2007	+2.28	0.09	11.03.2011	+5.20	0.20	10.07.2007
+4.79	0.27	12.06.2007	+2.89	0.18	20.06.2011	+4.93	0.12	25.07.2007
+4.87	*0.19*	21.06.2007	+2.73	0.28	01.09.2011	+5.08	0.95	25.07.2007
+4.76	0.20	10.07.2007	+2.50	0.43	18.03.2012	+4.93	0.12	25.09.2007
+4.84	0.16	26.09.2007	+2.64	0.20	12.06.2012	+4.76	0.22	29.10.2007
+4.73	0.22	17.10.2007	+2.60	0.49	03.09.2013	*+4.90*	*0.10*	29.10.2007
+4.67	0.29	26.09.2007	+2.53	0.26	11.08.2014	+4.86	0.20	30.01.2008
+4.57	0.04	14.01.2008	+2.74	0.28	09.09.2014	+5.00	0.20	28.02.2008
+4.73	*0.16*	14.01.2008	+2.73	0.18	18.05.2015	+4.88	0.17	20.06.2008
+4.73	0.20	21.06.2008				+4.95	0.25	20.06.2008
+4.82	0.56	22.10.2008				+4.68	0.14	22.10.2008
+4.70	0.40	15.12.2008				+4.83	0.08	03.11.2008
+4.73	0.17	29.03.2009				+4.89	0.23	12.11.2008
+4.58	0.20	07.04.2009				+4.57	0.44	02.02.2009
+4.59	0.30	10.06.2009				+4.98	0.23	03.03.2009
+4.74	0.21	27.11.2009				+4.77	0.31	27.11.2009
+4.39	0.29	23.03.2010				+4.94	0.22	19.01.2010
+4.43	0.23	19.04.2010				+4.87	0.34	08.12.2010
+4.70	0.23	26.07.2010				+4.65	0.05	17.05.2011
+4.81	0.19	04.07.2011						
+4.94	0.12	04.07.2011						
+4.84	0.21	16.09.2013						
+4.71	0.13	07.07.2014						
+4.73	0.25	mean (n = 36)	+2.59	0.31	mean (n = 22)	+4.91	0.31	mean (n = 32)

All analyses represent full individual chemical dissolution and cation-exchange separation, except for numbers shown in cursive, which are repeat mass spectrometer runs of previously analysed solutions.

reference materials run by this user are reported here and confirm a 0.3‰ (2SD) reproducibility for three different basalt reference materials run over nine years (Table S1). Despite the 0.3‰ reproducibility of standard data documented in both Jeffcoate *et al.* (2004) and Pogge von Strandmann *et al.* (2011) and the good agreement of their values of BHVO-2, Jeffcoate *et al.* (2004) reported a δ^7Li value for JB-2 0.5‰ lower than Pogge von Strandmann *et al.* (2011) and this study. In two-isotope systems it is difficult to determine which values are true, but there is clearly a user bias.

All samples are checked for imperfect collection of the Li fraction, ruling out a problem in chemical separation. So, perhaps the most probable cause of variability is in mass-spectrometer tuning and how this influences samples with small contrasts in residual matrix. The nature of residual matrices is poorly constrained, but an important difference between the samples analysed in Elliott *et al.* (2006) (and Jeffcoate *et al.*, 2004) and this study (and Pogge von Strandmann *et al.*, 2011) is that the former were processed with a mixed methanol-HNO_3/HCl chemistry, whereas here we used a dilute HCl chemistry.

Another possible cause of the poor reproducibility of some of the MORB samples is that they were hand-picked samples with as little as 2 mg of glass in some cases. The issue is not procedural blank as some samples originally analysed on large glass samples reproduce worse than those with less (cf PH64 for which 9 mg of glass was used, whereas only 2 mg was picked of PH77; Fig. S1). It is conceivable that picking was imperfect and minor amounts of alteration minerals were incorporated, which are typically enriched in Li and isotopically heavy. Although we believed the picking was robust this is hard to check in retrospect. It is also well documented that diffusive fractionation during eruptive cooling can fractionate Li during exchange with phenocrysts. Speculatively, the relative proximity of picked glass to rejected microphenocrysts might bias the result for small amounts of picked material. Unfortunately, none of these explanations provides a clear answer to the ultimate cause of the factor of two worse reproducibility between these two studies relative to the estimates from repeat analyses of a single user.

Fractional and batch melting models

The abundances of Li, B and the REE (Ce, Pr, Nd, Yb) were modelled using (i) a batch melting models, and (ii) a Rayleigh fractional melting model with accumulation of the extracted melt batches. Experimental mineral-melt partition coefficients were used, as listed in Table S2. The REE contents of the depleted mantle from Salters & Stracke (2004) are used for the melting protolith starting composition. Lithium and B contents of the protolith starting composition (= depleted mantle) are adjusted such that the Li/Yb and B/Pr ratios of the resulting melts generated by 2 to 20 % partial melting are within the range of target values of $\mathrm{Li/Yb} = 1.64 \pm 0.30$ and $\mathrm{B/Pr} = 0.57 \pm 0.10$.

Table S 2 Partition coefficients for trace elements employed for partial melting models

Data source	Lithium	Ytterbium	Boron	Cerium	Praseodymium	Neodymium
olivine						
McDade *et al.* (2003)	0.289	0.0096		$3.9*10^{-5}$	$9.0*10^{-5*}$	$2.1*10^{-4}$
Brenan *et al.* (1998)	0.35		0.008			
Ottolini *et al.* (2009)	0.427		0.008			
Chaussidon & Libourel (1993)			0.034			
Seitz (1973)			0.028			
Mean (employed here)	**0.355**	**0.0096**	**0.020**	**$3.9*10^{-5}$**	**$9.0*10^{-5}$**	**$2.1*10^{-4}$**
orthopyroxene						
McDade *et al.* (2003)	0.166	0.168		0.0047	0.0075*	0.012
Brenan *et al.* (1998)	0.20		0.018			
Ottolini *et al.* (2009)	0.211		0.024			
Chaussidon & Libourel (1993)			0.027			
Seitz (1973)			0.046			
Mean (employed here)	**0.192**	**0.168**	**0.029**	**0.0047**	**0.0075**	**0.012**
clinopyroxene						
McDade *et al.* (2003)	0.227	0.76		0.122	0.182*	0.273
Brenan *et al.* (1998)	0.27		0.025			
Ottolini *et al.* (2009)	0.246		0.041			
Chaussidon & Libourel (1993)			0.117			
Seitz (1973)			0.067			
Mean (employed here)	**0.248**	**0.76**	**0.063**	**0.122**	**0.182**	**0.273**
Bulk *D* (initial)	**0.289**	**0.151**	**0.027**	**0.017**	**0.026**	**0.039**

Note the large differences in partition coefficients for the REE among different minerals ($2-3$ orders of magnitude between olivine and clinopyroxene). In contrast, Li and B are more equally distributed with partition coefficients among the three major mantle minerals differing by approximately a factor of three or less. *the partition coefficients for Pr are arithmetic means of the respective Ce and Nd partition coefficients given by McDade *et al.* (2003) for each mineral–melt couple.

Table S 3 Results of partial melting models: 1. batch melting

F	Li	Yb	B	Ce	Pr	Nd	Li/Yb	B/Ce	B/Pr	B/Nd
Depleted Mantle, REE from Salters & Stracke (2004); Li and B are model input paramters										
	(1.20)	0.401	(0.077)	0.772	0.131	0.713	2.99	0.100	0.588	0.108
Melt composition										
0.01	4.024	2.545	2.082	28.903	3.727	14.895	1.581	0.072	0.559	0.140
0.02	3.899	2.448	1.649	21.313	2.950	12.560	1.593	0.077	0.559	0.131
0.03	3.781	2.357	1.366	16.881	2.440	10.857	1.604	0.081	0.560	0.126
0.04	3.670	2.274	1.165	13.974	2.081	9.562	1.614	0.083	0.560	0.122
0.05	3.565	2.196	1.016	11.922	1.814	8.542	1.624	0.085	0.560	0.119
0.06	3.466	2.123	0.901	10.395	1.608	7.719	1.633	0.087	0.560	0.117
0.07	3.373	2.055	0.809	9.215	1.444	7.041	1.641	0.088	0.561	0.115
0.08	3.284	1.991	0.734	8.275	1.301	6.472	1.650	0.089	0.561	0.113
0.09	3.200	1.931	0.672	7.509	1.199	5.988	1.657	0.090	0.561	0.112
0.10	3.120	1.874	0.620	6.874	1.105	5.572	1.665	0.090	0.561	0.111
0.12	2.972	1.771	0.536	5.878	0.956	4.891	1.678	0.091	0.561	0.110
0.15	2.774	1.635	0.446	4.829	0.794	4.134	1.697	0.092	0.561	0.108
0.20	2.497	1.450	0.348	3.722	0.620	3.286	1.722	0.094	0.561	0.106
0.25	2.270	1.302	0.286	3.028	0.509	2.727	1.743	0.094	0.561	0.105
Restite composition										
0.01	1.171	0.379	0.057	0.488	0.095	0.570	3.088	0.116	0.599	0.100
0.02	1.145	0.359	0.045	0.353	0.073	0.471	3.187	0.127	0.611	0.095
0.03	1.120	0.340	0.037	0.274	0.060	0.399	3.290	0.136	0.623	0.093
0.04	1.097	0.323	0.032	0.222	0.050	0.344	3.397	0.143	0.636	0.092
0.05	1.076	0.307	0.028	0.185	0.042	0.301	3.509	0.149	0.650	0.092
0.06	1.055	0.291	0.024	0.158	0.037	0.266	3.625	0.155	0.664	0.092
0.07	1.036	0.277	0.022	0.137	0.032	0.237	3.748	0.160	0.680	0.092
0.08	1.019	0.263	0.020	0.120	0.028	0.212	3.877	0.166	0.696	0.093
0.09	1.002	0.250	0.018	0.106	0.025	0.191	4.014	0.172	0.714	0.095
0.10	0.987	0.237	0.017	0.094	0.023	0.173	4.158	0.178	0.733	0.096
0.12	0.958	0.214	0.014	0.076	0.019	0.143	4.474	0.190	0.776	0.101
0.15	0.922	0.183	0.012	0.056	0.014	0.109	5.033	0.213	0.857	0.109
0.20	0.876	0.139	0.009	0.035	0.009	0.070	6.310	0.267	1.061	0.132
0.25	0.843	0.101	0.007	0.020	0.005	0.042	8.387	0.372	1.463	0.180

Trace element composition of extracted melt and restitic peridotite after batch melting were calculated using Equation S2 and Equation S3. REE contents of the DMM from Salters & Stracke (2004) were used as the starting composition.

Bulk partition coefficient D_{bulk} between the restitic whole rock and the extracted melts are determined from mineral-melt partition coefficients as

$$D_{\text{bulk}} = \sum(X_i D_i) \tag{1}$$

where D_i is the partition coefficient between mineral i and the melt, and X_i is the mass fraction of mineral i in the restitic rock. Mineral-melt partition coefficients for Li, B and the REE employed here are listed in Table S2. The depleted mantle modal composition of Workman & Hart (2005) was used for the starting composition of the depleted mantle with 57 % olivine, 28 % orthopyroxene, 13 % clinopyroxene, and 2 % spinel. Lithium, B and the REE were treated as perfectly incompatible ($D = 0$) in spinel. The abundances of Yb (0.401 µg/g), Ce (0.772 µg/g), Pr (0.131 µg/g) and Nd (0.713 µg/g) for the depleted mantle of Salters & Stracke (2004) were used (Table S3). The trace-element content of the liquid (c_L) extracted after batch melting is

$$c_{\text{L}} = \frac{c_0}{D_{\text{bulk}} + F(1-P)} \tag{2}$$

where c_0 is the initial concentration of the trace element in the rocks (= depleted mantle values in this case),

F is the degree of melting (0 to 1), and P is the bulk partition coefficient of the minerals that are dissolved into the melt. Following the low-pressure (1.1 GPa) melting model of Longhi (2002) the following proportions of dissolved minerals were used: −0.44 for olivine, 0.53 for orthopyroxene, 0.38 for clinopyroxene, and 0.53 for spinel, i.e., increase of the olivine mode and reduction of the pyroxene and spinel modes. The trace-element content of the restitic mantle rock (c_R) is

$$c_{\mathrm{R}} = \frac{c_0(D_{\mathrm{bulk}} - FP)}{(1-F)[D_{\mathrm{bulk}} + F(1-P)]} \tag{3}$$

Batch melting assumes that the trace-element content of the entire melt batch is equilibrated with the melt residue (the 'restite'). In contrast, fractional melting assumes that small melt batches are extracted consecutively until the target degree of melting is reached. These individual batches may in theory be infinitely small, in which case the Rayleigh fractionation formulation is applied. It is assumed that individually extracted melt batches are accumulated and homogenised. The trace-element content of the accumulated liquids (c_{L}) extracted by Rayleigh fractional melting is

Table S 4 Results of partial melting models: 2. Rayleigh fractional melting

F	Li	Yb	B	Ce	Pr	Nd	Li/Yb	B/Ce	B/Pr	B/Nd
Depleted Mantle, REE from Salters & Stracke (2004); Li and B are model input paramters										
	(1.20)	0.401	(0.077)	0.772	0.131	0.713	2.99	0.100	0.588	0.108
Melt composition										
0.01	4.090	2.596	2.373	34.400	4.248	16.341	1.576	0.069	0.559	0.145
0.02	4.023	2.542	2.015	26.942	3.594	14.630	1.583	0.075	0.561	0.138
0.03	3.957	2.488	1.728	21.577	3.066	13.134	1.590	0.080	0.563	0.132
0.04	3.893	2.436	1.495	17.666	2.640	11.827	1.598	0.085	0.566	0.126
0.05	3.830	2.384	1.306	14.769	2.294	10.684	1.607	0.088	0.569	0.122
0.06	3.768	2.332	1.151	12.586	2.011	9.684	1.616	0.091	0.573	0.119
0.07	3.708	2.281	1.024	10.911	1.780	8.809	1.625	0.094	0.575	0.116
0.08	3.649	2.231	0.918	9.601	1.588	8.043	1.635	0.096	0.578	0.114
0.09	3.591	2.182	0.829	8.557	1.429	7.371	1.646	0.097	0.580	0.112
0.10	3.535	2.133	0.754	7.712	1.296	6.780	1.657	0.098	0.582	0.111
0.12	3.425	2.037	0.636	6.432	1.088	5.803	1.681	0.099	0.585	0.110
0.15	3.269	1.898	0.512	5.147	0.873	4.721	1.722	0.099	0.587	0.108
0.20	3.029	1.681	0.385	3.860	0.655	3.563	1.802	0.100	0.588	0.108
0.25	2.812	1.481	0.308	3.088	0.524	2.852	1.898	0.100	0.588	0.108
Restite composition										
0.01	1.171	0.379	0.054	0.432	0.089	0.555	3.091	0.124	0.602	0.097
0.02	1.142	0.357	0.037	0.238	0.060	0.429	3.197	0.157	0.621	0.087
0.03	1.115	0.336	0.026	0.129	0.040	0.329	3.313	0.202	0.645	0.079
0.04	1.088	0.316	0.018	0.068	0.026	0.250	3.440	0.263	0.677	0.072
0.05	1.062	0.297	0.012	0.035	0.017	0.188	3.579	0.348	0.717	0.065
0.06	1.036	0.278	0.008	0.018	0.011	0.140	3.730	0.470	0.767	0.060
0.07	1.011	0.259	0.006	0.009	0.007	0.104	3.897	0.645	0.829	0.055
0.08	0.987	0.242	0.004	0.004	0.004	0.076	4.081	0.906	0.908	0.051
0.09	0.964	0.225	0.003	0.002	0.003	0.055	4.284	1.301	1.008	0.048
0.10	0.941	0.209	0.002	0.001	0.002	0.039	4.510	1.914	1.135	0.045
0.12	0.897	0.178	0.001	0.000	0.001	0.019	5.040	4.509	1.513	0.041
0.15	0.835	0.137	0.000	0.000	0.000	0.006	6.105	21.01	2.718	0.039
0.20	0.743	0.081	0.000	0.000	0.000	0.000	9.169	724.8	13.18	0.052
0.25	0.663	0.041	0.000	0.000	0.000	0.000	16.21	21900	251.5	0.158

Trace element composition of extracted melt and restitic peridotite after batch melting shown here were calculated using Equation S4 and Equation S5. REE contents of the DMM from Salters & Stracke (2004) were used as the starting composition.

$$c_{\mathrm{L}} = \frac{c_0}{F}\left[1-\left(1-\frac{FP}{D_{\mathrm{bulk}}}\right)^{\frac{1}{P}}\right] \tag{4}$$

and the trace-element content of the restitic mantle rock (c_{R}) in this case is

$$c_{\mathrm{R}} = \frac{c_0}{1-F}\left(1-\frac{FP}{D_{\mathrm{bulk}}}\right)^{\frac{1}{P}} \tag{5}$$

Results for trace-element modelling by batch melting are listed in Table S3 and for Rayleigh fractionation melting are given in Table S4.

Boron and Li compatibility

Figures 2 and 3 provide Li and B compatibility plots additional to the ones presented in the paper.

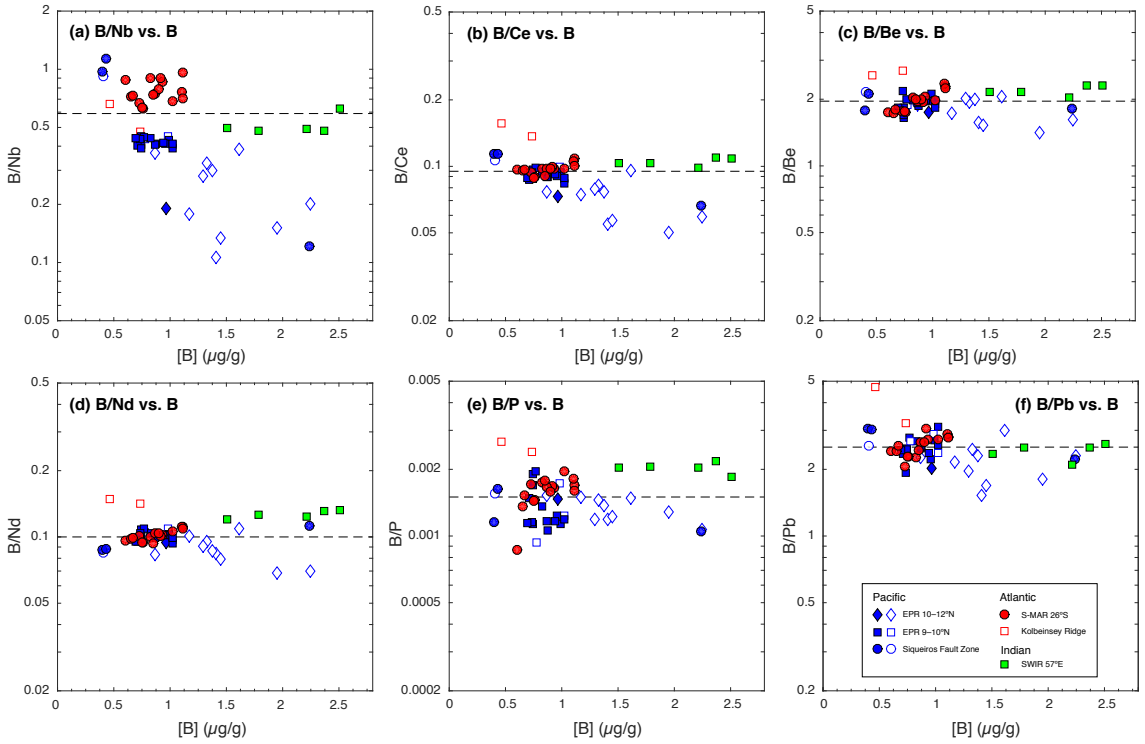

Fig. S 2 Boron/element ratios of MORB glasses analysed in this study. (a) B/K ratios vary widely among the samples and show a negative correlation with [B]. In contrast, (b) B/Ce, (c) B/Be, (d) B/Nd, (e) B/P, and (f) B/Pb ratios are relatively constant and do not show systematic variations with [B].

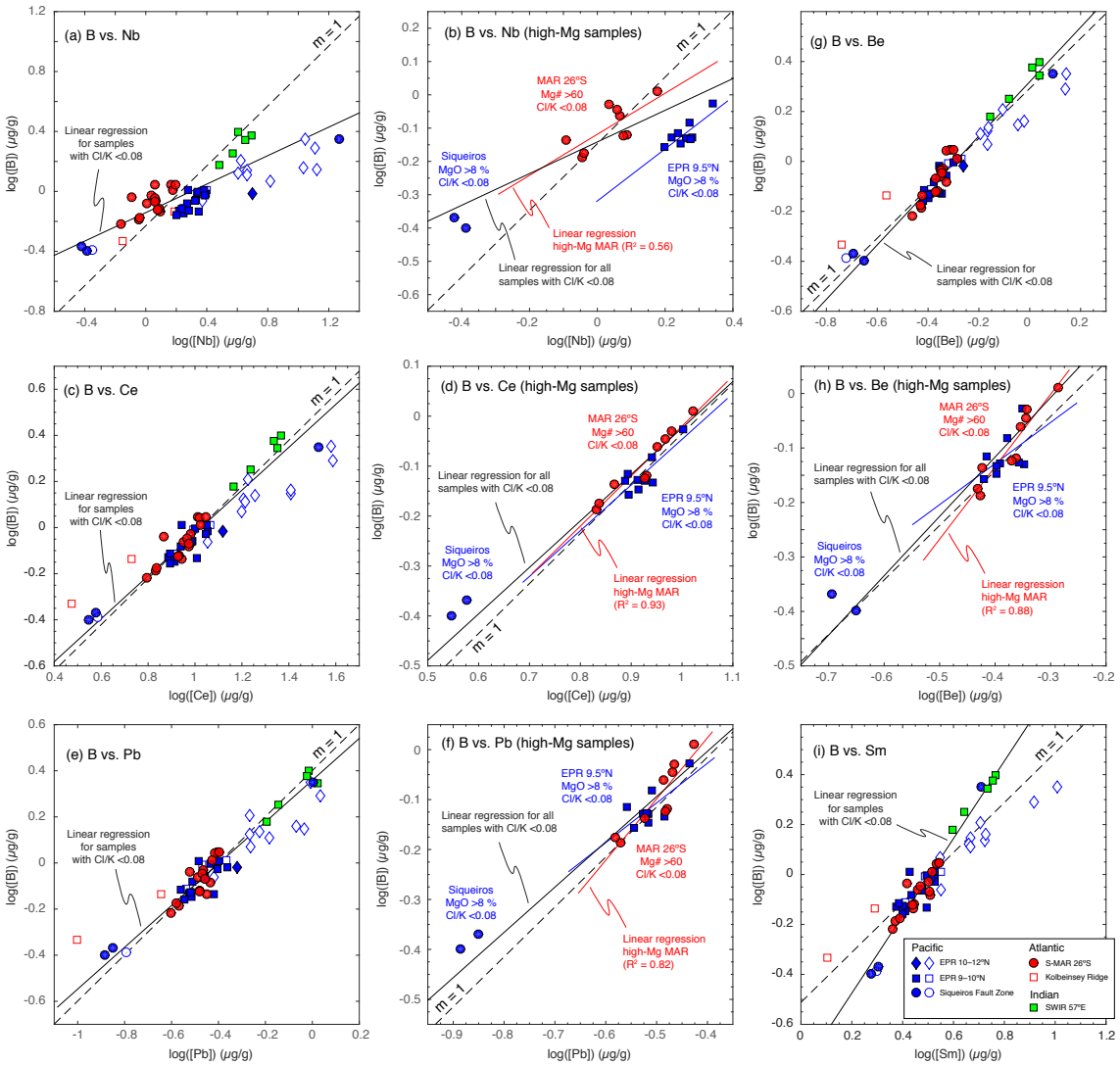

Fig. S 3 (a) Log-log plot (base 10) of [B] vs. [Nb] of all investigated samples, and (b) of samples with Mg# > 60 or MgO > 8 wt%, which establishes the relative compatibilities during MORB melting. The slopes of the linear regression lines of the subset of samples with low Cl/K (black line) are less than 1 (dashed line), showing that B behaves less incompatible than Nb on a global scale. The regression line of the high-Mg samples from an individual ridge section, MAR-26°S, also has a slope of less than 1, showing that B is less incompatibel than Nb during MORB melting; (c, d) Ce; (e, f) Pb; (g, h) Be; (i) Sm.

Trace element signature of investigated samples

Fig. S4 shows multi-element plots ("spidergrams") of all MORB glasses investigated in this study. Negative anomalies of Li and B are observed in all samples, with the exception of the two Kolbeinsey Ridge samples, which do not show B anomalies. The strongest anomalies are observed for chlorine. This, and the position of B next to Ce, P, Be and Pb, i.e. the order of the elements on the x-axis, are discussed in the paper.

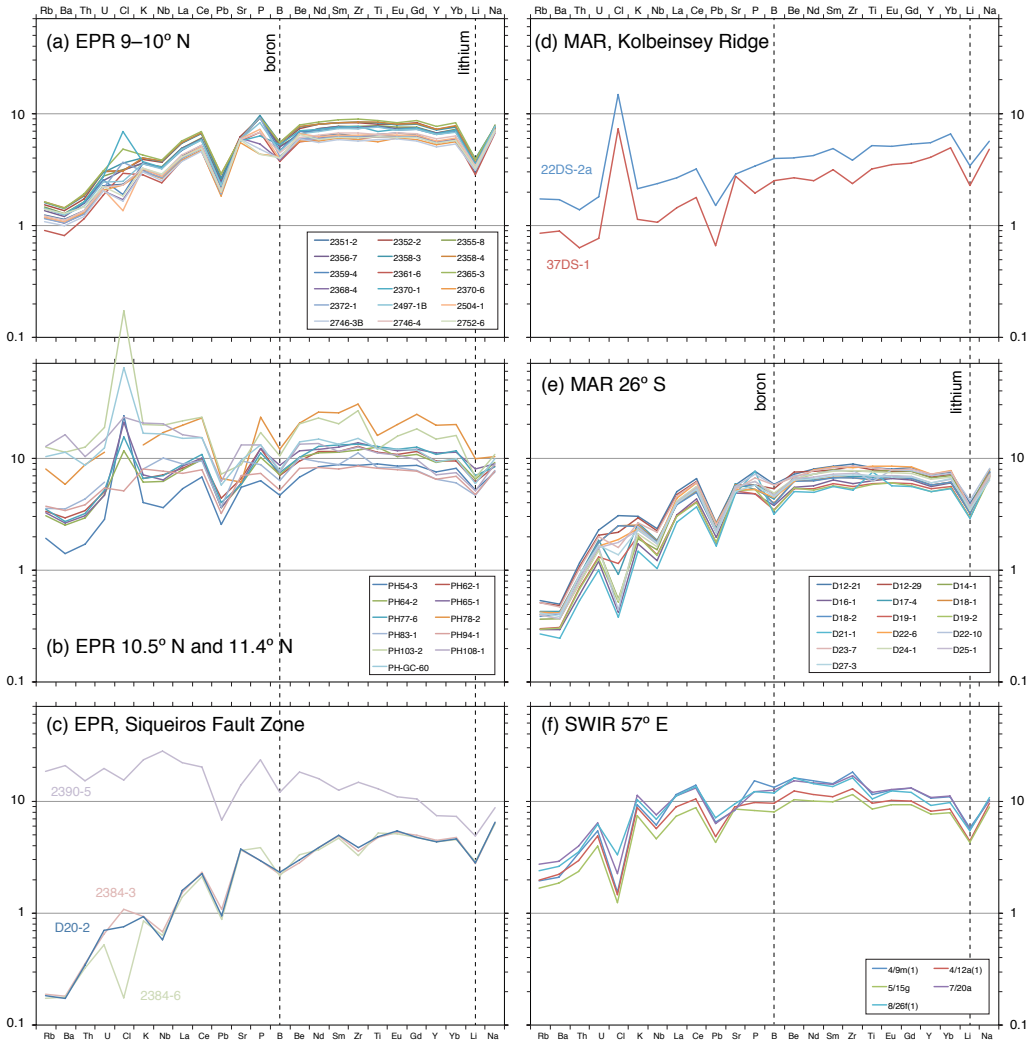

Fig. S 4 Multi-element plots ("spidergrams") of the MORB glasses investigated in this study from the six different ridge segments described in the paper. Li, B and all other trace-element data are from this study, except for a small number of published chlorine data. Element concentrations are normalised to primitive mantle abundances and displayed in order of decreasing incompatibility during mantle melting. The primitive mantle abundance estimates of Li and B from this study are used (see main paper), whereas estimates from McDonough & Sun (1995) were used for all other elements.

Lithium and boron equilibrium isotope fractionation in magmatic systems?

Tomascak *et al.* (1999) investigated a series of glasses from the Kilauea Iki lava lake (Hawai'i) and concluded that no resolvable Li isotope fractionation occurred during fractional crystallisation of olivine over a large range in MgO contents and temperatures between 1216 to 1050 °C. Their analytical precision (2σ) was ± 1.1‰. The same conclusion of no resolvable Li isotope fractionation during fractional crystallisation was reached by Halama *et al.* (2007) for differentiating alkali basalts and carbonatites, and by Schuessler *et al.* (2009) through the investigation of a series of basalts to dacites from Hekla volcano (Iceland), with an external reproducibility of their method of ± 0.5‰. Jeffcoate *et al.* (2007) investigated olivine–melt Li isotope fractionation by analysing olivine phenocrysts and the groundmass or glass from lava flow samples from Hawai'i and Iceland equilibrated between 900 and 1100 °C, and they found that the phenocrysts were less than 0.5‰ higher in δ^7Li than the groundmass or glass. The authors conclude from these findings that the Li isotopic composition of mantle-derived melts are $0.2-0.5$‰ lower in δ^7Li than their mantle source (Jeffcoate *et al.*, 2007).

Equilibrium Li isotope fractionation is dominantly driven by differences in the coordination environment of the Li ions in the coexisting phases (e.g., Jahn & Wunder, 2009). Strong Li isotope fractionation is observed, for example, between clinopyroxene and hydrous fluid, where Li is in octahedral and tetrahedral coordination, respectively. Wunder *et al.* (2006) quantified the systematic, temperature-dependent fractionation between clinopyroxene and fluid experimentally, and an extrapolation of their calibration to magmatic conditions would predict a fractionation of 0.55‰ at 1250 °C and 0.36‰ at 1350 °C. Melt–mantle fractionation would only follow this fractionation line, if Li coordination in the melt would also be tetrahedral, as it is in hydrous fluids. For octahedral coordination of Li in the melt, no measurable Li isotope fractionation would be expected between silicate melt and mantle minerals.

Clearly, more experimental data is needed to determine the Li isotope fractionation between basaltic melt and coexisting minerals, but realistically a fractionation of less than 0.5‰ at 1250 °C is expected, and this value may be used to model the maximum effects of fractional crystallisation on Li isotopes in basalts. Similarly, a value of less than 0.35‰ at 1350 °C may be used to model partial melting in the mantle.

Boron isotope fractionation is largest between phases that show different coordination of B with O, i.e. trigonal and tetrahedral coordination, respectively (e.g., Palmer & Swihart, 1996). Coordination of B in basaltic melts is not known, but other natural silicate melts have been shown to contain a minor fraction of tetrahedral B ($8-26$% of the total B; Tonarini *et al.*, 2003). Ferromagnesian silicates are likely dominated by B in tetrahedral coordination in substitution for Si or tetrahedral Al; however, it has been demonstrated that B incorporation in clinopyroxene and olivine may lead to a change in the local structure in these minerals with trigonal coordination of B (Hålenius *et al.*, 2010; Ingrin *et al.*, 2014). The mixed trigonal and tetrahedral coordination environments in both basaltic melts and silicate minerals suggests that B isotope fractionation between solids and liquid during partial melting of the mantle and during fractional crystallisation is smaller than the fractionation predicted for phases with exclusively trigonal and tetrahedral fractionation, respectively.

Natural obsidian glass with biotite phenocrysts were used by Tonarini *et al.* (2003) to determine B isotope fractionation of $6.6-2.8$‰ at magmatic temperatures of $780-860$ °C. Experiments between basaltic melt and hydrous fluid at temperatures of $750-1100$ °C showed a B isotope fractionation of $7.1-1.3$‰ (Hervig *et al.*, 2002). Extrapolation of the observations from these two studies to temperatures of 1250 °C and 1350 °C predicts a B isotope fractionation of 2.6 and 2.1‰, respectively, using a linear regression of the relation between $1000\ln\alpha$ and $1/T^2$ that is zero at infinite temperature.

Sanchez-Valle *et al.* (2005) used vibrational spectroscopy to determine boron isotope fractionation between minerals and fluids at high temperatures. They parametrised their data, which allows them to predict B isotope fractionation between 3- and 4-coordinated sites in minerals, fluids and melts at a given tempera-

ture. For example, at 1250 °C the fractionation is expected to be 2.4‰, and at 1350 °C the fractionation is expected to be 2.1‰. In the case of fractionation between mantle minerals and basaltic melt, and between crystallising silicates and basaltic melt, the fractionation should be significantly smaller, since coordination is not exclusively trigonal or tetrahedral in the phases involved, as argued above.

Clearly, more experimental data is needed to determine the B isotope fractionation between basaltic melt and coexisting minerals, but it can be expected that B isotope fractionation is less than 1.0‰ at 1250 °C, relevant for fractional crystallisation of basaltic liquids, and an upper limit of 0.9‰ may be estimated for partial melting in the mantle at 1350 °C. The melt is estimated to be enriched in the heavy isotope, i.e., it is higher in δ^{11}B than the solids.

Equilibrium stable isotope fractionation of Li and B during partial melting of the mantle may be modelled as modal batch melting, where the Li isotopic composition of the restitic rock is:

$$\delta^7\mathrm{Li}_\mathrm{R} = \frac{\delta^7\mathrm{Li}_0 \cdot c_0 - 1000F \cdot \frac{c_\mathrm{L}}{\alpha - 1}}{(1-F)c_\mathrm{R} + F \cdot \frac{c_\mathrm{L}}{\alpha}} \tag{6}$$

where α is the stable isotope fractionation factor and $\delta^7\mathrm{Li}_0$ is the isotopic composition of the initial rock. An equivalent equation applies to B isotope fractionation. The isotopic composition of the extracted melt can be calculated from the isotopic composition of the rock (from Equation S6) employing the isotope fractionation factor:

$$\delta^7\mathrm{Li}_\mathrm{L} = \frac{\delta^7\mathrm{Li}_\mathrm{R} + 1000}{\alpha} - 1000 \tag{7}$$

Equilibrium isotope fractionation and element partition coefficients between basaltic liquid and the restitic peridotite were used to estimate the maximum effect of equilibrium isotope fractionation. The solid–melt bulk partition coefficients used in our model are 0.027 for B and 0.289 for Li (Table S2) for this simple modal batch melting model for the mantle and for fractional crystallisation of MORB. For Li we adopt a fractionation of 0.55‰ at 1250 °C to model the effects of fractional crystallisation, and a value of 0.36‰ at 1350 °C to model partial melting in the mantle. For B we use a fractionation of 1.0‰ at 1250 °C to model the effects of fractional crystallisation, and 0.9‰ at 1350 °C to model partial melting in the mantle.

These isotope fractionation values are regarded as upper limits for the possible magnitude of equilibrium Li and B isotope fractionation, and the results of the model should only be interpreted as a first-order estimate of the possible effect of partial melting on the fractionation of Li and B isotopes between MORB and its mantle source. Further input parameters for the model are the element abundances of the mantle, and the Li and B isotopic composition of MORB estimated in this study. The model results show that basaltic melts (primitive or differentiated) have δ^7Li and δ^{11}B values within 0.4‰ of their mantle sources.

Published lithium abundances in mantle peridotite samples

A growing number of studies have reported Li abundances in lherzolite and harzburgite xenoliths hosted in alkali basalts and kimberlites, and from one orogenic peridotite massif. The reported Li whole-rock concentrations range from 0.5 to 15 µg/g (Fig. S5). The samples also show a range of Yb contents that correlate positively with Al_2O_3 contents, and both elements systematically decrease from the primitive-mantle value observed in fertile lherzolites to values near zero in refractory harzburgites (Fig. S5d). Lithium does not show such a correlation with indicators of melt extraction, such as Mg# or Al_2O_3 content (Fig. S5a,b). Many samples were interpreted by the authors as metasomatised by fluids or melts in the mantle or by the host magma during eruption; they show elevated Li contents in excess of 2 µg/g and strongly elevated Li/Yb ratios (Fig. S5f).

Geochemical indicators of metasomatism include elevated K_2O contents, elevated light REE contents relative to the medium and heavy REE, and disturbed Li isotope compositions. Samples that show any of these characteristic traits of secondary processes must be excluded from a discussion of Li abundances in the primitive and depleted mantle and of the behaviour of Li during melting of the mantle. The subset of samples that show low K_2O contents (< 0.05 wt%), flat or depleted normalised REE patterns and δ^7Li values between $+2.5$ and $+6.0$‰ (or for which no Li isotope values are available) are displayed in Fig. S6.

The patterns are similar to the ones described above for the full dataset, but with less scatter and lower maximum Li abundances. Most samples show [Li] between 1 and 2 µg/g, with the exception of samples from two localities for which no Li isotope values are available (Fig. S6a-c). This reduced set of samples

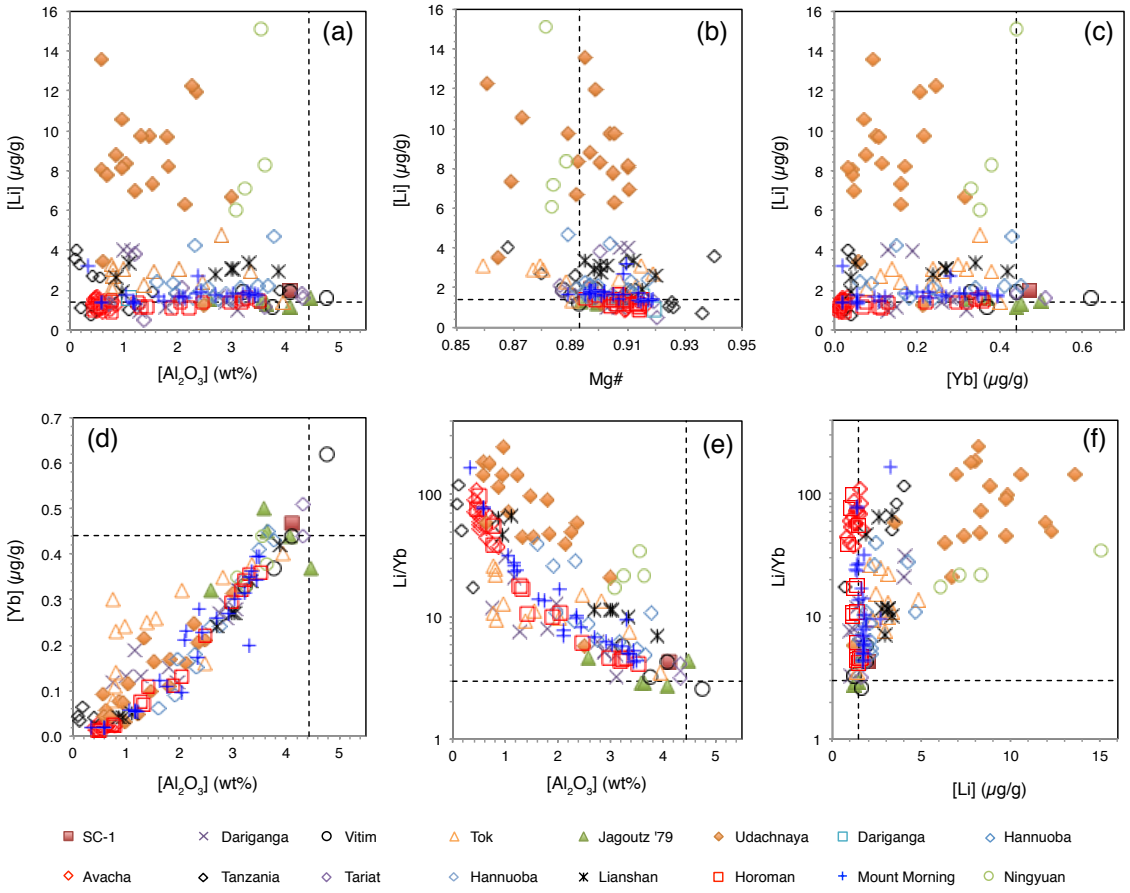

Fig. S 5 Compilation of published data on mantle xenoliths and the Horoman orogenic peridotite for which whole-rock Li data is available. Primitive mantle Mg# (= molar Mg/(Mg + Fe)) and abundances of Yb and Al_2O_3 are from McDonough & Sun (1995), whereas the primitive mantle Li abundance (1.39 µg/g) is from this study. The primitive mantle abundances and element ratios are marked by the dashed lines. Data sources are: SC1 (San Carlos): Seitz *et al.* (2004); Jagoutz'79 (five samples, various localities): Jagoutz *et al.* (1979); Avacha (Kamchatka): Ionov & Seitz (2008); Vitim, Tariat, Tok and Dariganga x (Mongolia and Lake Baikal region of Russia): Pogge von Strandmann *et al.* (2011); Dariganga, squares (Mongolia): Magna *et al.* (2008); Udachnaya (Siberia): Agashev *et al.* (2013); Mount Mourning (East Antarctica): Martin *et al.* (2015); Tanzania: Aulbach & Rudnick (2009); Hannuoba, light blue diamonds (North China Craton): Tang *et al.* (2007); Hannuoba, dark blue diamonds: Rudnick *et al.* (2004); Ningyuan (south-eastern China): Zhang *et al.* (2008); Lianshan (eastern China): Lu *et al.* (2012); Horoman Massif (Japan): Lai *et al.* (2015).

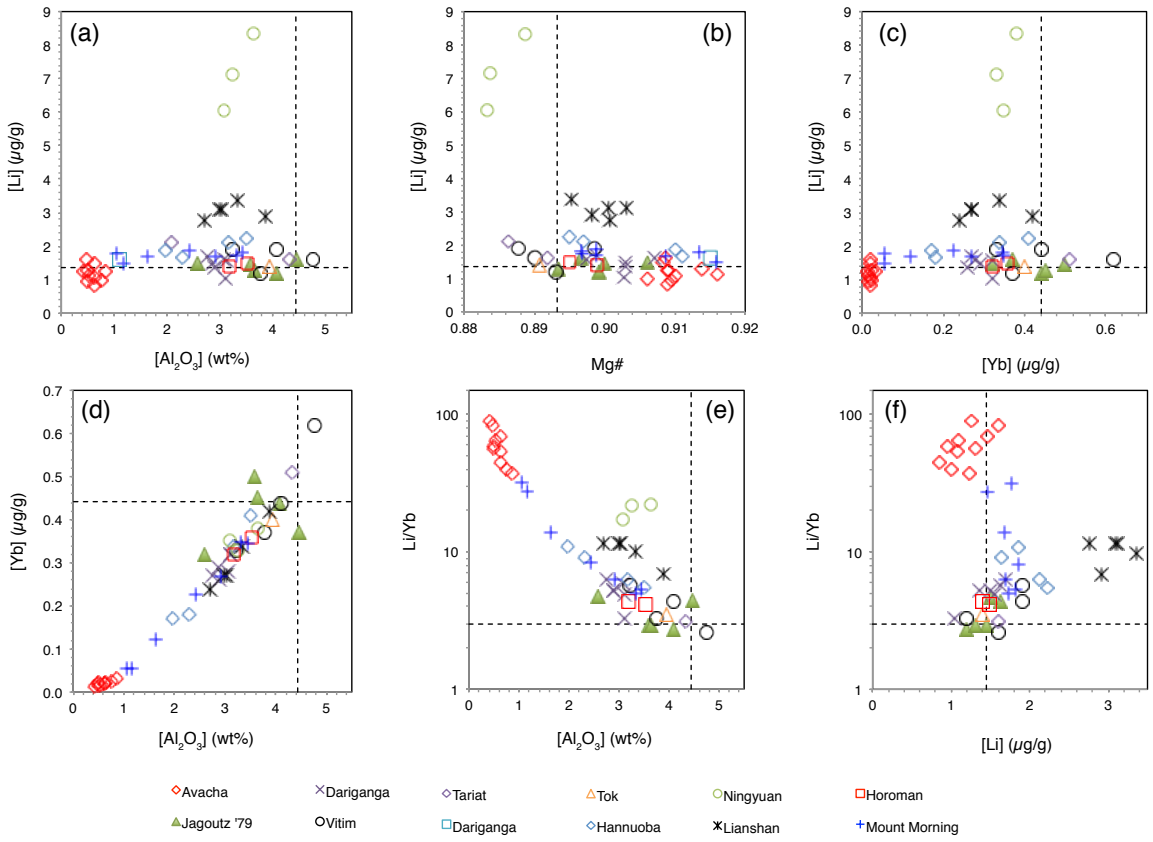

Fig. S 6 Compilation of a selected subset of samples displayed in Fig. S5. Selection criteria discriminated against samples that show obvious signs of metasomatism and excluded samples that showed the following: (i) $K_2O > 0.05\,\%$, (ii) $\delta^7Li < +2.5‰$ or $\delta^7Li > +6.0‰$, and (iii) CI-normalised REE pattern that show enrichment of the light REE or that show S- or spoon-shaped patterns. Note that no Li isotope data were available for the samples from Mount Mourning, Ningyuan, Hannuoba, Lianshan, some of the Avacha samples and the samples from Jagoutz *et al.* (1979); these samples may hence viewed with more caution. See Fig. S5 for data sources.

may, therefore, still contain some metasomatised samples. The selected sample set still does not show a correlation of Li contents with indicators of melt depletion, but the systematic decrease in Yb contents with decreasing Al_2O_3 leads to a strong increase of Li/Yb ratios with decreasing Al_2O_3 (Fig. S6e). This observation is consistent with the results of the melting models presented above, which predict Li/Yb to increase from 2.99 ± 0.25 for the depleted mantle to values above 5 or even above 10 for very high degrees of melt depletion (Table S3 and Table S4). Lithium contents of highly depleted mantle predicted from the melting models are still $\sim 50-70\,\%$ of the contents of the primitve mantle (Table S3 and Table S4), and similarly the set of natural samples do not show a drastic decrease in Li with melt depletion (Fig. S6a-c).

Lithium isotope fractionation by diffusion

Lithium isotope fractionation was modelled theoretically to test whether it is feasible to produce Li isotope excursions of approximately 1‰ in bulk basaltic liquids by kinetic fractionation. The model assumes a semi-infinite magma chamber in contact to a semi-infinite host rock. The Li concentration in the melt

and the host rock are randomly set to 5 µg/g and 1 µg/g, respectively, and the equilibrium bulk partition coefficient for Li between host rock and melt is 0.289 (Table S2). The Li concentration in the melt is, therefore, approximately 145 % of the concentration that would be in equilibrium with the host rock (i.e., 3.5 µg/g). A chemical potential gradient of this magnitude could be induced, for example, by the contrast in pressure or temperature between the magma source region and the magma chamber, or by changes in the

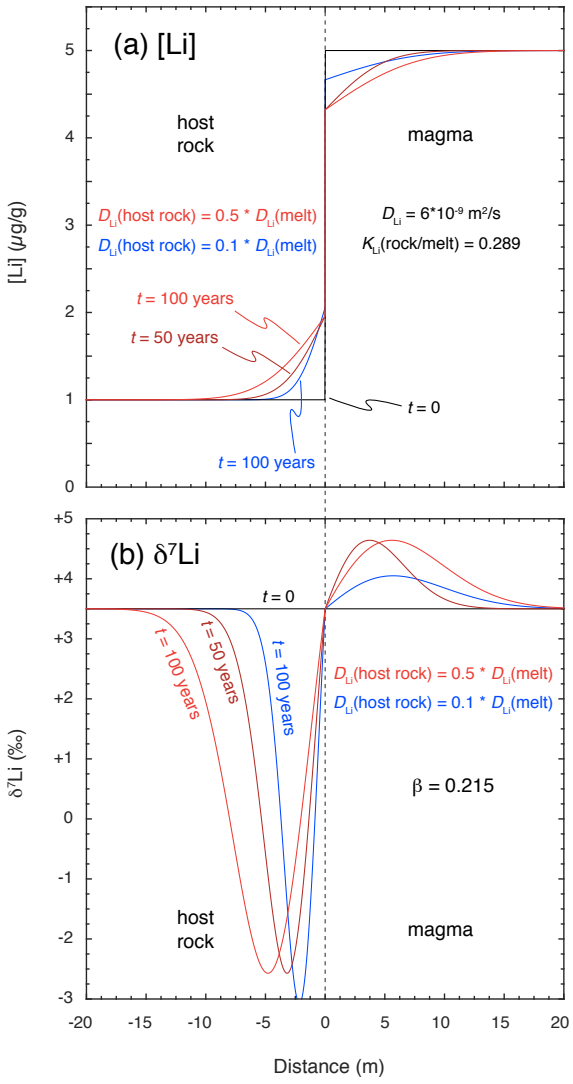

Fig. S 7 Graphic display of results of 1-dimensional diffusion model for (a) Li concentrations and (b) Li isotopes between a magma body (right) and its host rock (left) at high temperature ($T = 1350\,^{\circ}$C). Three stages of a time series from $t = 0$ (black) to $t = 50$ years (dark red) to $t = 100$ years (bright red) are shown for a scenario in which the diffusion coefficient of Li in the host rock is half as high as in the magma. The blue line depicts the results of a diffusion model in which the Li diffusion coefficient in the host rock is only 10 % of the one in the magma. The positive excursions produced in the magma are approximately 10 m wide after 100 years with amplitudes of approximately 0.5 ‰ (blue line) and 1.1 ‰ (red lines).

modal composition of the host rock, or by partial crystallisation of the magma. A homogenous initial Li isotopic composition is assumed with δ^7Li $= +3.5$‰ in both magma and host rock (Fig. S7).

Lithium diffusion was modelled separately for the two isotopes, and the δ^7Li was determined from the resulting diffusion profiles. The analytical solution of diffusion in one dimension with non-unity Li equilibrium partitioning between melt and host rock and with two different diffusion coefficients for Li in melt and host rock, respectively, was used (modified after Crank, 1975, his equations 3.45 and 3.46):

$$C_{\text{melt}} = -C_{\text{rock, 0}} + \frac{C_{\text{melt, 0}} - C_{\text{rock, 0}}}{1 + K\sqrt{D_{\text{rock}}/D_{\text{melt}}}} \left(1 + K\sqrt{D_{\text{rock}}/D_{\text{melt}}} \cdot erf \frac{x}{2\sqrt{D_{\text{melt}} t}}\right), \tag{8}$$

and

$$C_{\text{rock}} = C_{\text{rock, 0}} + \frac{K(C_{\text{melt, 0}} - C_{\text{rock, 0}})}{1 + K\sqrt{D_{\text{rock}}/D_{\text{melt}}}} \cdot erfc \frac{|x|}{2\sqrt{D_{\text{rock}} t}}, \tag{9}$$

where C_{melt} and C_{rock} are the concentrations of Li in the melt and the host rock, respectively. $C_{\text{melt, 0}}$ and $C_{\text{rock, 0}}$ are the initial concentrations of Li in the melt and the host rock at time $t = 0$, respectively. D_{melt} and D_{rock} are the Li diffusion coefficients in the melt and the host rock, respectively. K is the bulk equilibrium partition coefficient for Li between host rock and melt, and t is time. The distance x from the host rock–melt contact has positive values in the melt and negative values in the host rock (see Fig. S7). The diffusion coefficient of Richter *et al.* (2003) for Li diffusion in basaltic liquid at 1350°C ($D = 6 * 10^{-9}$ m^2/s) was used for ^{6}Li diffusion in the melt, as well as a kinetic fractionation exponent beta = 0.215, to determine the diffusion coefficient of the heavier isotope ^{7}Li (Richter *et al.*, 2003). A range of diffusion coefficients D_{rock} were used to test the effect of this parameter on kinetic isotope fractionation.

The model predicts a diffusive enrichment of Li in the host rock and a depletion of Li in the magma within approximately 10 m of the contact after 100 years (Fig. S7a). Faster diffusion of ^{6}Li leads to kinetic fractionation of the Li isotopes. The country rock shows excursions to negative δ^7Li values of approximately -2 to -3‰ (Fig. S7b). The kinetically favoured preferential loss of ^{6}Li from the melt leads to a concurrent rise of δ^7Li in the melt in the vicinity of the contact. The amplitude of the kinetically induced Li isotope anomaly does not depend on time (yet their width and positions do), but it depends on the relative diffusivity of Li in host rock and magma (as well as on Li partitioning, on initial Li concentrations, and on β). The amplitudes are approximately 0.2‰ for $D_{\text{rock}}/D_{\text{melt}} = 0.01$ (not shown), 0.5‰ for $D_{\text{rock}}/D_{\text{melt}} = 0.1$, and 1.1‰ for $D_{\text{rock}}/D_{\text{melt}} = 0.5$ (Fig. S7b).

The example presented here demonstrates that it may be possible to generate excursions of 1‰ in δ^7Li as observed in the EPR 9.5°N section (see main paper) by kinetic fractionation in a time span of decades. The exact amount of fractionation obviously depends on the geometric parameters, the difference in chemical potential of Li between melt and country rock, and the diffusion parameters (D and β). Convection in the magma chamber would homogenise the Li isotope excursions of the marginal region with its unfractionated interior part and dampen the anomalous isotope signal. In contrast, small magma chambers or dykes that have larger surface to volume ratios may produce even more extreme isotope excursions.

Lithium, B and radiogenic isotopes in MORB

In addition to the figures presented in the paper, Figures 8 and 9 provide a full compilation of Li and B isotopes with the radiogenic systems of Sr, Nd and Pb. Neodymium isotope ratios for EPR $9-10$°N and the Siqueiros Fault Zone samples from Sims *et al.* (2002) were recalculated based on a CHUR ^{143}Nd/^{144}Nd = 0.51262 to be consistent with the other literature values.

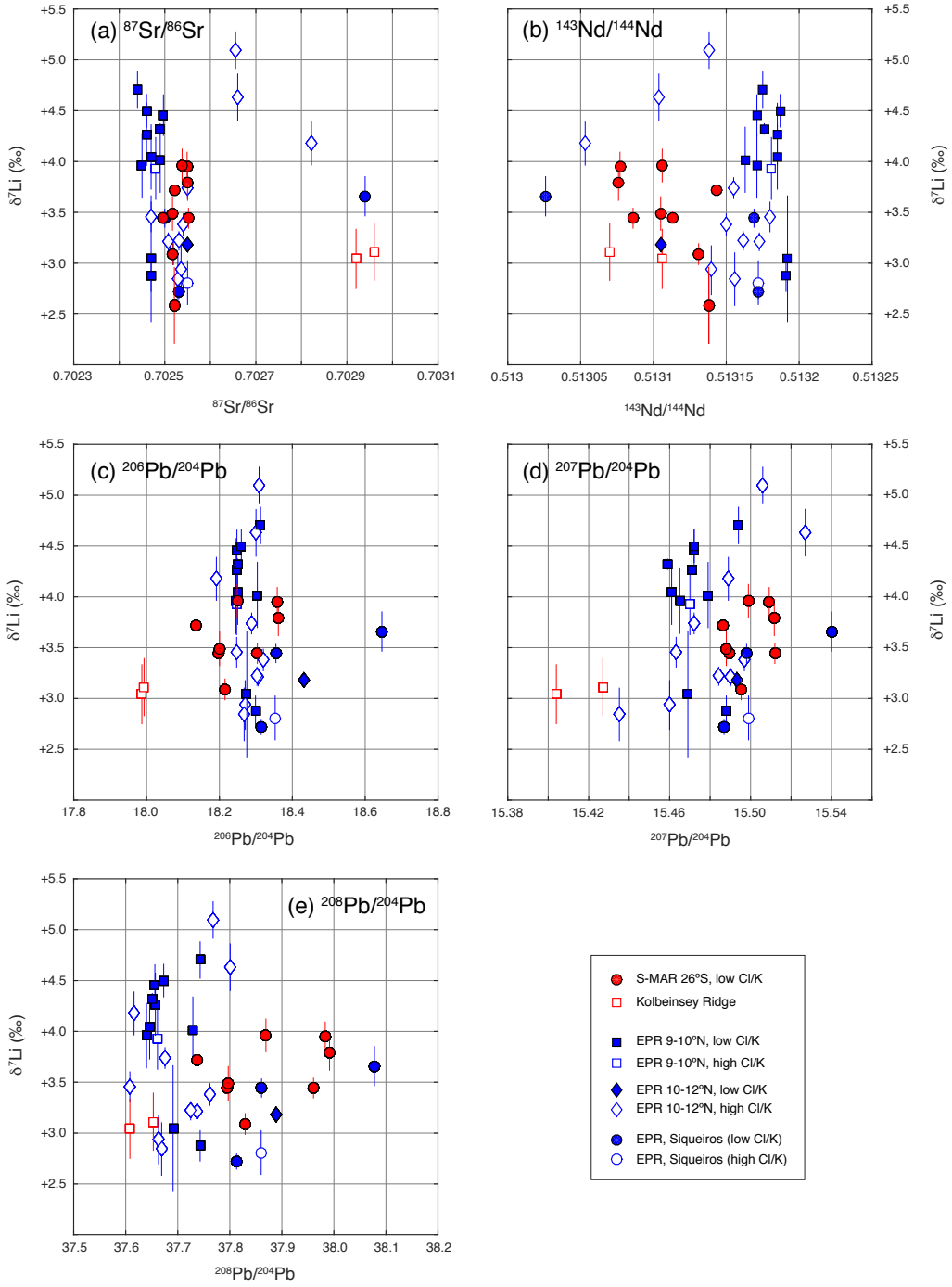

Fig. S 8 Lithium isotopic composition of MORB glass samples plotted vs. radiogenic isotopes of Sr, Nd and Pb. Lithium isotopes do not vary systematically with radiogenic isotopes. (a) $^{87}Sr/^{86}Sr$; (b) $^{143}Nd/^{144}Nd$; (c) $^{206}Pb/^{204}Pb$; (d) $^{207}Pb/^{204}Pb$; (e) $^{208}Pb/^{204}Pb$.

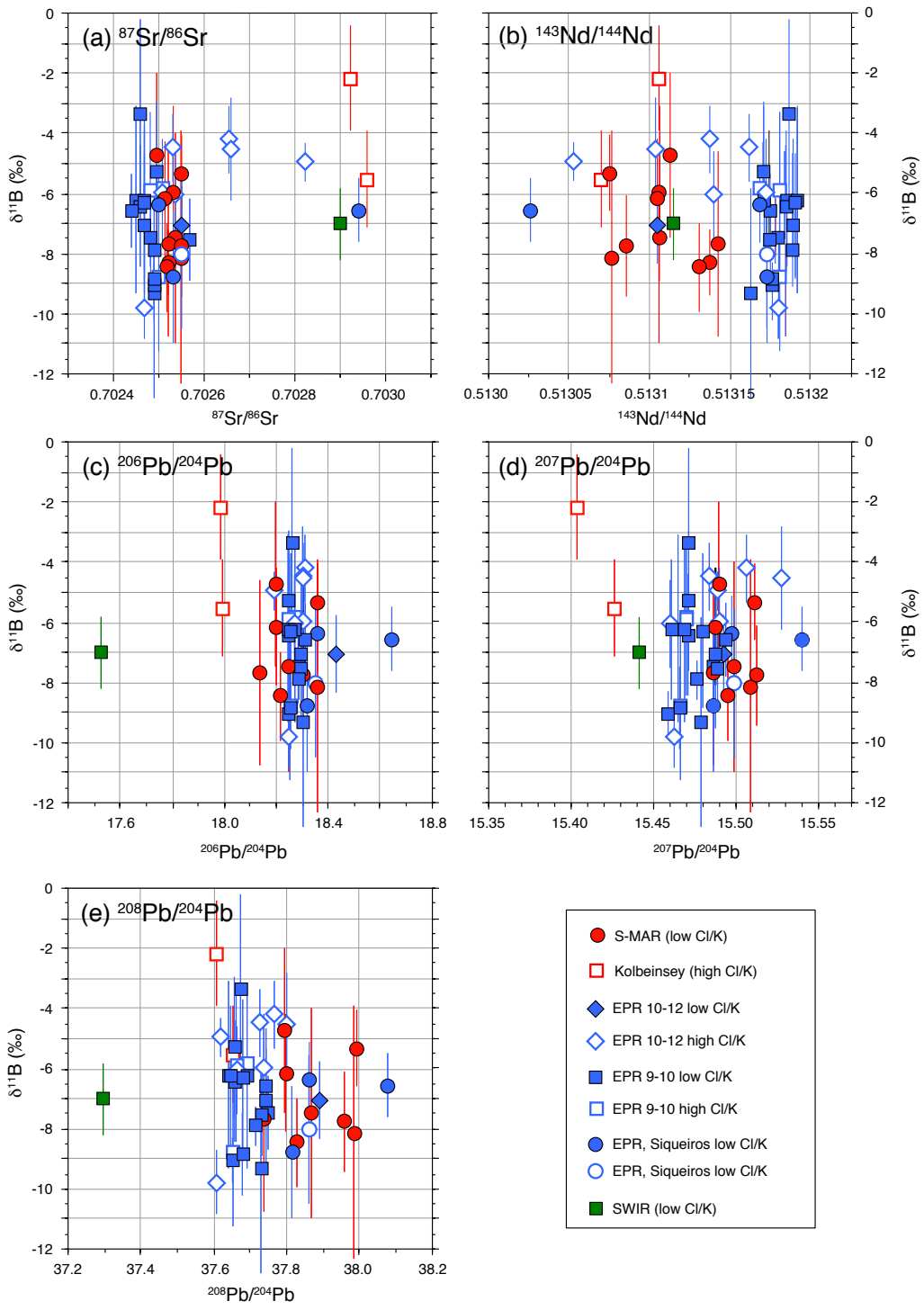

Fig. S 9 Boron isotopic composition of MORB glass samples plotted vs. radiogenic isotopes of Sr, Nd and Pb. Boron isotopes do not vary systematically with radiogenic isotopes. (a) $^{87}Sr/^{86}Sr$; (b) $^{143}Nd/^{144}Nd$; (c) $^{206}Pb/^{204}Pb$; (d) $^{207}Pb/^{204}Pb$; (e) $^{208}Pb/^{204}Pb$.

Seafloor sample maps

Bathymetric maps with sample localities on the MAR 26°S, the EPR, and the SWIR are presented with samples colour coded for MgO contents.

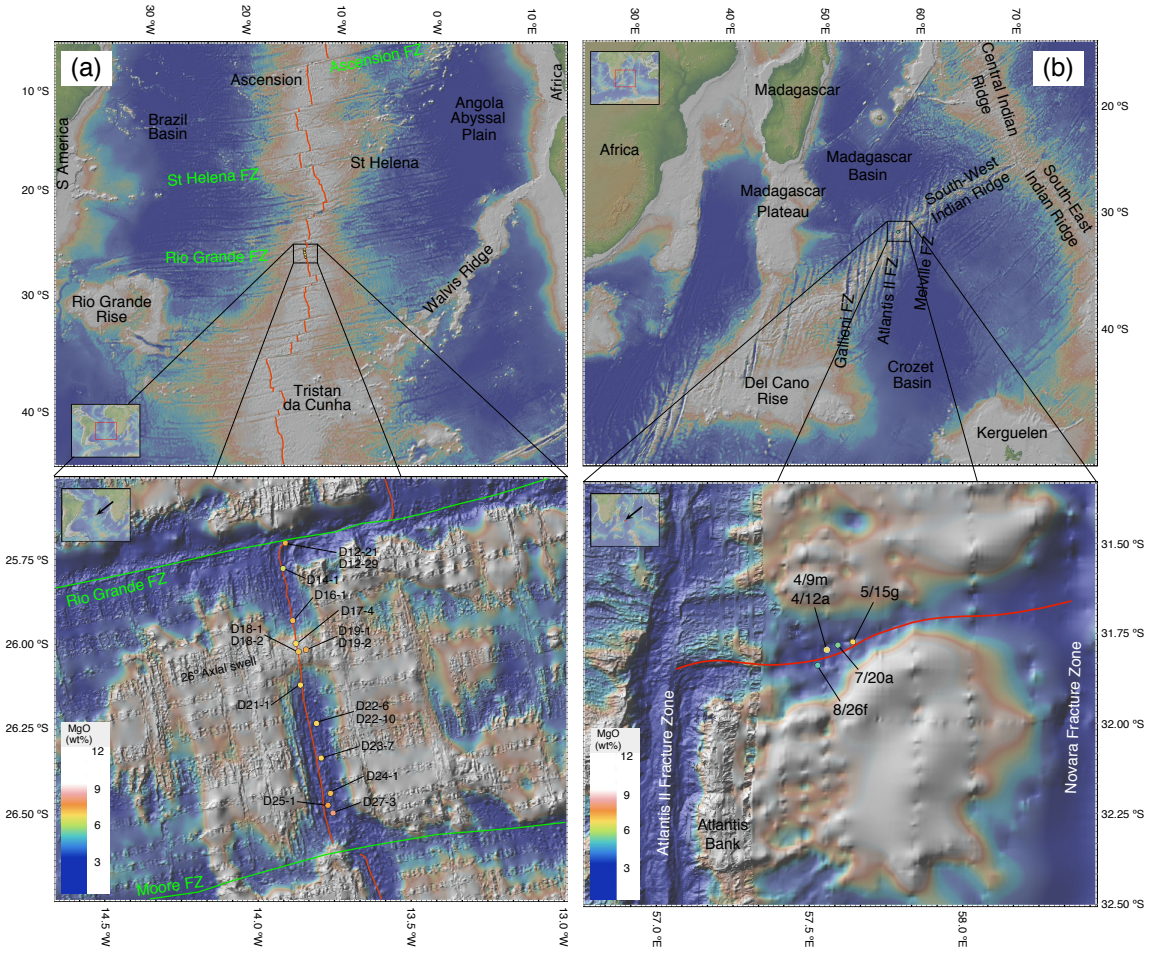

Fig. S 10 Maps with sample locations on the **(a)** southern Mid-Atlantic Ridge and **(b)** South-West Indian Ridge. The upper panels show the ocean basins and ridges with the sample areas outlined in black, which are zoomed in on in the lower panels. Sample localities are marked in the lower panels by circles and colour coded according to the MgO content of the volcanic glass (see colour scale on the left side). Maps were generated in GeoMapApp (http://www.geomapapp.org/) using the Global Multi-Resolution Topography synthesis base map (Ryan *et al.*, 2009). Map colours refer to bathymetry with warm colours marking shallow seafloor and cold colours marking deep seafloor.

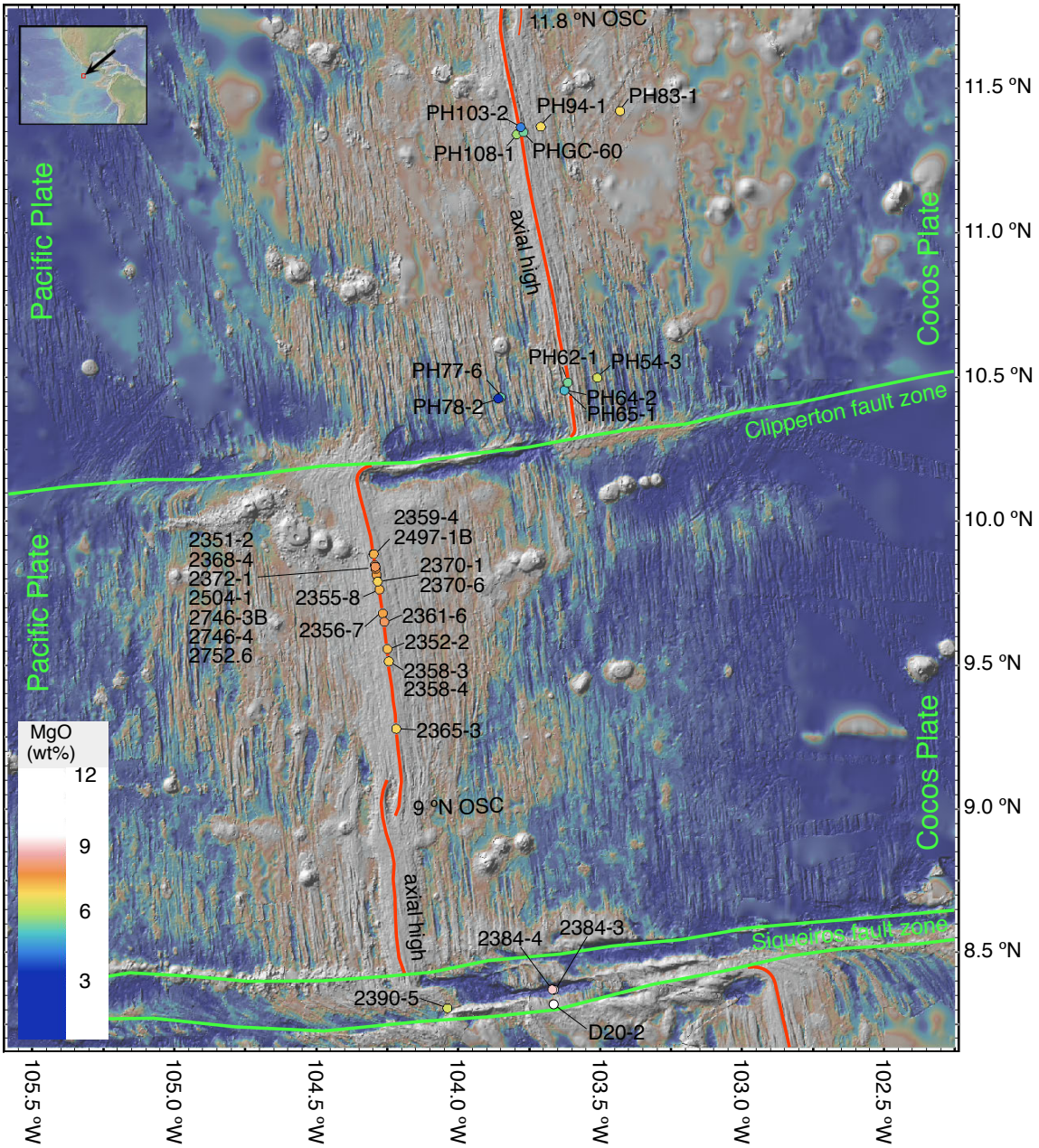

Fig. S 11 Map with samples from EPR generated in GeoMapApp (http://www.geomapapp.org/) using the Global Multi-Resolution Topography synthesis base map (Ryan *et al.*, 2009). Samples were selected from two across-axis profiles at 10.5°N and 11.2°N, respectively. A set of 18 samples are from the ridge axis between 9°N and 10°N, and three samples come from the Siqueiros fault zone. Sample localities are marked by circles and colour coded according to the MgO content of the volcanic glass (see colour scale on the left side). OSC = overlapping spreading center.

References

Agashev, A. M., Ionov, D. A., Pokhilenko, N. P., Golovin, A. V., Cherepanova, Y. & Sharygin, I. S. (2013) Metasomatism in lithospheric mantle roots: constraints from whole-rock and mineral chemical composition of deformed peridotite xenoliths from kimberlite pipa Udachnaya. *Lithos* **160**: 201–215

Aulbach, S. & Rudnick, R. L. (2009) Origins of non-equilibrium lithium isotopic fractionation in xenolithic peridotite minerals: examples from Tanzania. *Chemical Geology* **258**: 17–27

Brenan, J. M., Neroda, E., Lundstrom, C. C., Shaw, H. F., Ryerson, F. J. & Phinney, D. L. (1998) Behavior of boron, beryllium and lithium during melting and crystallization: constraints from mineral-melt partitioning experiments. *Geochimica et Cosmochimica Acta* **62**: 2129–2141

Chaussidon, M. & Libourel, G. (1993) Boron partitioning in the upper mantle: an experimental and ion microprobe study. *Geochimica et Cosmochimica Acta* **57**: 5053–5062

Crank, J. (1975) *The Mathematics of Diffusion*. Oxford University Press, Oxford, 2^{nd} edn.

Elliott, T., Thomas, A., Jeffcoate, A. & Niu, Y. (2006) Lithium isotope evidence for subduction-enriched mantle in the source of mid-ocean-ridge basalts. *Nature* **443**: 565–568

Halama, R., McDonough, W. F., Rudnick, R. L., Keller, J. & Klaudius, J. (2007) The Li isotopic composition of Oldoinyo Lengai: nature of the mantle sources and lack of isotopic fractionation during carbonatite petrogenesis. *Earth and Planetary Science Letters* **254**: 77–89

Hålenius, U., Skogby, H., Edén, M., Nazzareni, S., Kristionsson, P. & Resmark, J. (2010) Coordination of boron in nominally boron-free rock forming silicates: Evidence for incorporation of BO_3 groups in clinopyroxene. *Geochimica et Cosmochimica Acta* **74**: 5672–5679

Hervig, R. L., Moore, G. M., Williams, L. B., Peacock, S. M., Holloway, J. R. & Roggensack, K. (2002) Isotopic and elemental partitioning of boron between hydrous fluid and silicate melt. *American Mineralogist* **87**: 769–774

Ingrin, J., Kovács, I., Deloule, E., Balan, E., Blanchard, M., Kohn, S. C. & Hermann, J. (2014) Identification of hydrogen defects linked to boron substitution in synthetic forsterite and natural olivine. *American Mineralogist* **99**: 2138–2141

Ionov, D. A. & Seitz, H. M. (2008) Lithium abundances and isotopic compositions in mantle xenoliths from subduction and intra-plate settings: mantle sources vs. eruption histories. *Earth and Planetary Science Letters* **266**: 316–331

Jagoutz, E., Palme, H., Baddenhausen, H., Blum, K., Cendales, M., Dreibus, G., Spettel, B., Lorenz, V. & Wänke, H. (1979) The abundances of major, minor and trace elements in the Earth's mantle as derived from primitive ultramafic nodules. *Proceedings of the 10^{th} Lunar and Planetary Science Conference* 2031–2050

Jahn, S. & Wunder, B. (2009) Lithium speciation in aqueous fluids at high P and T studied by ab initio molecular dynamics and consequences for Li-isotope fractionation between minerals and fluids. *Geochimica et Cosmochimica Acta* **73**: 5428–5434

Jeffcoate, A. B., Elliott, T., Thomas, A. & Bouman, C. (2004) Precise, small sample size determinations of lithium isotopic compositions of geological reference materials and modern seawater by MC-ICP-MS. *Geostandards And Geoanalytical Research* **28**: 161–172

Jeffcoate, A. B., Elliott, T., Kasemann, S. A., Ionov, D., Cooper, K. & Brooker, R. (2007) Li isotope fractionation in peridotites and mafic melts. *Geochimica et Cosmochimica Acta* **71**: 202–218

Lai, Y. J., Pogge von Strandmann, P. A. E., Dohmen, R., Takazawa, E. & Elliott, T. (2015) The influence of melt infiltration on the Li and Mg isotopic composition of the Horoman Peridotite Massif. *Geochimica et Cosmochimica Acta* **164**: 318–332

Longhi, J. (2002) Some phase equilibrium systematics of lherzolite melting: I. *Geochemistry, Geophysics, Geosystems (G^3)* **3**: 10.1029/2001GC000 204

Lu, J., Zheng, J., Griffin, W. L. & Yu, C. (2012) Petrology and geochemistry of peridotite xenoliths from the Lianshan region: nature and evolution of lithospheric mantle beneath the lower Yangtze block. *Gondwana Research* **23**: 161–175

Magna, T., Ionov, D. A., Oberli, F. & Wiechert, U. (2008) Links between mantle metasomatism and lithium isotopes: evidence from glass-bearing and cryptically metasomatized xenoliths from Mongolia. *Earth and Planetary Science Letters* **276**: 214–222

Martin, A. P., Price, R. C., Cooper, A. F. & McCammon, C. A. (2015) Petrogenesis of the rifted Southern Victoria Land lithospheric mantle, Antarctica, inferred from petrography, geochemistry, thremobarometry and oxybarometry of peridotite and pyroxenite xenoliths from the Mount Mourning eruptive centre. *Journal of Petrology* **56**: 193–226

McDade, P., Blundy, J. D. & Wood, B. J. (2003) Trace element partitioning between mantle wedge peridotite and hydrous MgO-rich melt. *American Mineralogist* **88**: 1825–1831

McDonough, W. F. & Sun, S. S. (1995) The composition of the Earth. *Chemical Geology* **120**: 223–253

Ottolini, L., Laporte, D., Raffone, N., Devidal, J. L. & Le Fèvre, B. (2009) New experimental determination of Li and B partition coefficients during upper mantle partial melting. *Contributions to Mineralogy and Petrology* **157**: 313–325

Palmer, M. R. & Swihart, G. H. (1996) Boron isotope geochemistry: an overview. In: Grew, E. S. & Anovitz, L. M. (eds.) *Boron: mineralogy, petrology and geochemistry*, vol. 33 of *Reviews in Mineralogy*, chap. 13, 709–740, Mineralogical Society of America, Washington, DC, 1^{st} edn.

Richter, F. M., Davis, A. M., DePaolo, D. J. & Watson, E. B. (2003) Isotope fractionation by chemical diffusion between molten basalt and rhyolite. *Geochimica et Cosmochimica Acta* **67**: 3905–3923

Rudnick, R. L., Gao, S., Ling, W. L., Liu, Y. S. & McDonough, W. F. (2004) Petrology and geochemistry of spinel peridotite xenoliths from Hannuoba and Qixia, North China craton. *Lithos* **77**: 609–637

Ryan, W. B. F., Carbotte, S. M., Coplan, J. O., O'Hara, S., Melkonian, A., Arko, R., Weissel, R. A., Ferrini, V., Goodwillie, A., Nitsche, F., Bonczkowski, J. & Zemsky, R. (2009) Global Multi-Resolution Topography synthesis. *Geochemistry, Geophysics, Geosystems (G^3)* **10**: Q03 014

Salters, V. J. M. & Stracke, A. (2004) Composition of the depleted mantle. *Geochemistry, Geophysics, Geosystems (G^3)* **5**: 10.1029/2003GC000 597

Sanchez-Valle, C., Reynard, B., Daniel, I., Lecuyer, C., Martinez, I. & Chervin, J. C. (2005) Boron isotope fractionation between minerals and fluids: New insights from in-situ high pressure-high temperature vibrational spectroscopic data. *Geochimica et Cosmochimica Acta* **69**: 4301–4313

Schuessler, J. A., Schoenberg, R. & Sigmarsson, O. (2009) Iron and lithium isotope systematics of the Hekla volcano, Iceland – evidence for Fe isotope fractionation during magma differentiation. *Chemical Geology* **258**: 78–91

Seitz, H. M., Brey, G. P., Lahaye, Y., Durali, S. & Weyer, S. (2004) Lithium isotopic signatures of peridotite xenoliths and isotopic fractionation at high temperature between olivine and pyroxenes. *Chemical Geology* **212**: 163–177

Seitz, M. G. (1973) Boron mapping and partitioning in synthetic and natural systems: crystal-melt assemblages, garnet lherzolite, chondrites. *Carnegie Institution Washington Yearbook* **72**: 588–593

Sims, K. W. W., Goldstein, S. J., Blichert-Toft, J., Perfit, M. R., Keleman, P. B., Fornari, D. J., Michael, P. J., Murrell, M. T., Hart, S. R., DePaolo, D. J., Layne, G., Ball, L., Jull, M. & Bender, J. (2002) Chemical and isotopic constraints on the generation and transport of magma beneath the East Pacific Rise. *Geochimica et Cosmochimica Acta* **66**: 3481–3504

Pogge von Strandmann, P. A. E., Elliott, T., Marschall, H. R., Coath, C., Lai, Y. J., Jeffcoate, A. & Ionov, D. A. (2011) Variations of Li and Mg isotope ratios in bulk chondrites and mantle xenoliths. *Geochimica et Cosmochimica Acta* **75**: 5247–5258

Tang, Y. J., Zhang, H. F., Nakamura, E., Moriguti, T., Kobayashi, K. & Ying, J. F. (2007) Lithium isotopic systematics of peridotite xenoliths from Hannuoba, North China Craton: implications for melt-rock interaction in the considerably thinned lithospheric mantle. *Geochimica et Cosmochimica Acta* **71**: 4327–4341

Tomascak, P. B., Tera, F., Helz, R. T. & Walker, R. J. (1999) The absence of lithium isotope fractionation during basalt differentiation: new measurements by multicollector sector ICP-MS. *Geochimica et Cosmochimica Acta* **63**: 907–910

Tonarini, S., Forte, C., Petrini, R. & Ferrara, G. (2003) Melt/biotite $^{11}B/^{10}B$ isotopic fractionation and the boron local environment in the structure of volcanic glasses. *Geochimica et Cosmochimica Acta* **67**: 1863–1873

Workman, R. K. & Hart, S. R. (2005) Major and trace element composition of the depleted MORB mantle (DMM). *Earth and Planetary Science Letters* **231**: 53–72

Wunder, B., Meixner, A., Romer, R. L. & Heinrich, W. (2006) Temperture-dependent isotopic fractionation of lithium between clinopyroxene and high-pressure fluids. *Contributions to Mineralogy and Petrology* **151**: 112–120

Zhang, H. F., Goldstein, S. L., Zhou, X. H., Sun, M., Zheng, J. P. & Cai, Y. (2008) Evolution of subcontinental lithospheric mantle beneath eastern China: Re-Os isotopic evidence from mantle xenoliths in Paleozoic kimberlites and Mesozoic basalts. *Contributions to Mineralogy and Petrology* **155**: 271–293